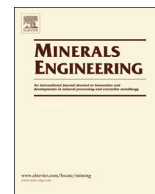




ELSEVIER

Contents lists available at ScienceDirect

Minerals Engineering

journal homepage: [www.elsevier.com/locate/mineng](http://www.elsevier.com/locate/mineng)

## Sulfidization mechanism in malachite flotation: A heterogeneous solid-liquid reaction that yields $\text{Cu}_x\text{S}_y$ phases grown on malachite

Ruizeng Liu<sup>a</sup>, Dianwen Liu<sup>a,b,\*</sup>, Jialei Li<sup>a,\*</sup>, Jianmin Li<sup>c</sup>, Zhicheng Liu<sup>d</sup>, Xiaodong Jia<sup>a</sup>, Shengwang Yang<sup>a</sup>, Jiangli Li<sup>a</sup>, Shuai Ning<sup>a</sup>

<sup>a</sup> Faculty of Land Resources Engineering, Kunming University of Science and Technology, Kunming 650093, Yunnan, PR China

<sup>b</sup> State Key Laboratory of Complex Nonferrous Metal Resources Clean Utilization, Kunming 650093, Yunnan, PR China

<sup>c</sup> Northwest Research Institute of Mining and Metallurgy, Baiyin 730900, Gansu, PR China

<sup>d</sup> Chihong Technology & Engineering Co. Ltd, Qujing, Yunnan 655000, PR China



### ARTICLE INFO

#### Keywords:

Malachite  
Copper oxide ores  
Flotation  
Sulfidization  
Copper sulfide

### ABSTRACT

Sulfidization followed by xanthate flotation is an effective technique to recover copper oxide minerals. However, the sulfidization mechanism of malachite has not been determined. In this work, the sulfidization mechanism was investigated by microflotation, field emission scanning electron microscopy (FESEM), energy dispersive spectroscopy (EDS), electron probe X-ray microanalysis (EPMA), X-ray diffraction (XRD) and X-ray photoelectron spectroscopy (XPS). The flotation results showed that sulfide ions at an appropriate concentration could activate malachite flotation while excess sulfide ions could depress this. The depression of malachite flotation by excess sulfide ions was attributed to the residual sulfide species in the liquid. FESEM-EDS showed that sulfidization product grown on the malachite surface was heterogeneously distributed, which was consistent with the EPMA results. The XRD results for the sulfidized malachite samples showed that the amount of sulfidization product was insufficient for detection under flotation-related conditions. By the selective solvent action of sulfuric acid, the sulfidization product was extracted from the sulfidized malachite. The XRD results for the extracts indicated that the sulfidization product comprised djurleite ( $\text{Cu}_{31}\text{S}_{16}$ ) and anilite ( $\text{Cu}_7\text{S}_4$ ), which both were compounds of the chalcocite group ( $\text{Cu}_{2-x}\text{S}$ ), suggesting transformation of solid  $\text{Cu}_2(\text{OH})_2\text{CO}_3$  to  $\text{Cu}_{2-x}\text{S}$  on the malachite surfaces during sulfidization. Moreover, the XPS results were consistent with the XRD results. These results demonstrated that sulfidization of malachite is a phase-transition process driven by the solubility difference between  $\text{Cu}_2(\text{OH})_2\text{CO}_3$  and  $\text{Cu}_{2-x}\text{S}$ . In this case,  $\text{Cu}_{2-x}\text{S}$  phases formation on malachite involves heterogeneous nucleation and growth, and sulfide ions act as a reductant and sulfidizing agent in malachite sulfidization. The copper sulfide grown on malachite radically changed the surface properties of malachite particles, rendering malachite amenable to xanthate flotation. Based on these findings, we present a new formula for malachite sulfidization and a schematic diagram of the sulfidized malachite particle.

### 1. Introduction

Copper, a vital non-ferrous metal, has significantly influenced the history of civilization, especially in the bronze age. This metal is now enmeshed in every aspect of present-day life because of its remarkable malleability, good resistance to corrosion and excellent electrical and thermal conductivity. In nature, copper usually occurs as copper sulfide minerals. Chalcopyrite ( $\text{CuFeS}_2$ ), bornite ( $\text{Cu}_5\text{FeS}_4$ ) and chalcocite ( $\text{Cu}_2\text{S}$ ) are the three most important copper minerals, accounting for the majority of copper resources on Earth (Thompson and Base, 2006; Li et al., 2013). With increased sulfide resource depletion, the utilization of low-grade oxide ores has received increasing attention in recent

years. Copper oxide minerals, such as malachite ( $\text{Cu}_2(\text{OH})_2\text{CO}_3$ ), azurite ( $\text{Cu}_3(\text{CO}_3)_2(\text{OH})_2$ ), tenorite ( $\text{CuO}$ ) and cuprite ( $\text{Cu}_2\text{O}$ ), are oxidized products of copper sulfide at the earth's surface (Thompson and Base, 2006). Compared with copper sulfide minerals, oxide minerals are difficult to directly float due to their hydrophilic surfaces when using conventional sulfide mineral collectors. A representative method for recovering copper oxide minerals is sulfidization followed by flotation with xanthate.

Sulfidization converts oxide mineral surfaces to more hydrophobic sulfide compounds, which renders the mineral particles amenable to xanthate flotation. Sulfidization can be achieved by directly adding sulfidizing agents into pulp, or with the aid of mechanochemical,

\* Corresponding authors at: Faculty of Land Resources Engineering, Kunming University of Science and Technology, Kunming 650093, PR China (D. Liu).

E-mail addresses: [dianwenliu@kmust.edu.cn](mailto:dianwenliu@kmust.edu.cn) (D. Liu), [lijialei1993@foxmail.com](mailto:lijialei1993@foxmail.com) (J. Li).

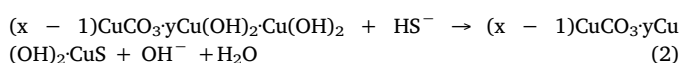
<https://doi.org/10.1016/j.mineng.2020.106420>

Received 11 September 2019; Received in revised form 14 March 2020; Accepted 1 May 2020

0892-6875/© 2020 Elsevier Ltd. All rights reserved.

hydrothermal or roasting methods (Wang et al., 2003; Han et al., 2014; Ke et al., 2015). A higher degree of sulfidization can be acquired using the latter three methods; however, these methods are normally used for processing wastes containing heavy metals and inappropriate for treating naturally formed ores, due to their high cost, high-energy consumption and specific equipment requirements. Therefore, the first method is considered to be the most viable and economical approach.

The origin of sulfidization–flotation can be traced back to the early parts of the last century, but detailed studies of sulfidization in the flotation of copper oxide minerals were performed until the 1970s. Castro et al. (1974) suggested that sulfidization of tenorite is a complex multiple reaction involving three major steps: (1) adsorption of sulfide with formation of a copper sulfide layer; (2) sulfide oxidation; and (3) desorption of oxidized compounds according to an ion-exchange mechanism. In addition, covellite was found in a sulfidized tenorite sample by X-ray diffraction (XRD). In the subsequent work, Bustamante and Castro (1975) proposed Eqs. (1) and (2) to explain the activation of sodium sulfide on malachite flotation. However, the reaction path and products were only hypothetical. Based on Eq. (2), Zhou and Chander (1993) proposed Eq. (3) as the initial step in sulfidization to explain the formation of colloidal copper particles in the liquid. They suggested that besides some of the malachite forming a CuS coating, the dissolved copper ions might precipitate as copper sulfide or hydrolyze to copper hydroxide to form colloidal particles. For decades, CuS was generally recognized as the sulfidization product of malachite in most literature, including textbooks, regardless of the form of the sulfidization reaction. However, Liu (2007) observed the XRD peaks of Cu<sub>7</sub>S<sub>4</sub> (roxbyite) when 0.5 g of malachite was treated with excess sodium sulfide ( $1 \times 10^{-1}$  mol/L), but found no diffraction peaks of sulfide when the sodium sulfide concentration ( $1 \times 10^{-3}$  mol/L) was the most suitable for flotation. X-ray photoelectron spectroscopy (XPS) studies conducted by Feng et al. (2017) showed that the sulfur species on malachite surfaces comprised monosulfide, disulfide and polysulfide, and some Cu(II) ions were reduced to Cu(I). Nevertheless, the crystal phase of sulfidization product could not be determined from the XPS data.



Surprisingly, data gaps still exist concerning the properties of sulfidization product of malachite under flotation-related conditions, including the morphology, chemical composition, crystal phase and distribution on the mineral surface. Because the sulfidization product is unknown, the reaction path remains unclear. That is, the sulfidization mechanism in the flotation of malachite has not yet been determined. Thus, previous studies on sulfidization flotation of malachite were also limited by the lack of information on the sulfidization reaction, e.g., the role and mechanism of ammonium and ethylenediamine in the malachite sulfidization remain poorly understood.

This work attempted to further elucidate the sulfidization mechanism of malachite and lay a foundation for future research. Microflotation tests, electron probe X-ray microanalysis (EPMA), field emission scanning electron microscopy (FESEM), energy dispersive spectroscopy (EDS), XRD and XPS were performed. These results provide a deeper understanding of the sulfidization mechanism of malachite.

## 2. Materials and methods

### 2.1. Materials

A pure malachite sample obtained from Kunming, China was crushed in a laboratory double-roll crusher and dry ground in an agate mortar. The ground products were then sieved to obtain particles with sizes of 37–74 μm for use in this work. After treatment, the purity of the powder sample was 98.1% based on chemical analysis.

NaOH and HCl were selected as pH regulators, and Na<sub>2</sub>S·9H<sub>2</sub>O was employed as a sulfidizing agent. Sulfuric acid was applied as a leaching agent, and ascorbic acid served as antioxidant in the extraction of the sulfidization product. The aforementioned compounds were all of analytical purity (AR) grade. Industry-grade sodium butyl xanthate was purified to use as the collector. Deionized water (18.25 MΩ cm) was used in all experiments.

### 2.2. Flotation tests

To investigate the sulfidization–flotation behavior of malachite, batch flotation experiments were conducted in a 50 mL Hallimond tube using 5 mL/L nitrogen gas as flotation gas. In a flotation test, a 0.5 g powder sample and deionized water were placed in a beaker, which then was stirred for 1 min with a mechanical stirrer. Subsequently, the flotation reagents reagents were added to the pulp according to the respective experiment designs shown in Table 1. After treatment, the 50 mL of pulp was transferred to the Hallimond tube. After flotation for 10 min, the flotation recovery was calculated on the basis the dry weight of the floating and sunken material. Each flotation test was conducted at least thrice. The average value and standard deviation of each test are presented.

### 2.3. FESEM-EDS analyses

Sulfidization of the samples for all characterizations methods was the same: First, 0.5 g of malachite sample was stirred with deionized water for 1 min. Na<sub>2</sub>S solution with a desired concentration was then added to the pulp. After agitating for 3 min, the treated malachite sample was washed with deionized water thrice and dried in a vacuum dryer.

The morphologies of unsulfidized and sulfidized malachite samples were characterized by FESEM (Nova NanoSEM 450). EDS (Oxford X-Max) was used to analyze the chemical composition. Prior to analysis, the FESEM samples were coated with platinum.

**Table 1**  
Experimental procedures for flotation tests.

Parameter	Group	Experimental procedures
C(NaBX)	unsulfidized	String → pH adjustment → xanthate adsorption → flotation
	sulfidized	String → sulfidization → pH adjustment → xanthate adsorption → flotation
C(Na <sub>2</sub> S)	unwashed	String → sulfidization → pH adjustment → xanthate adsorption → flotation
	washed	String → sulfidization → wash → pH adjustment → xanthate adsorption → flotation
Ultrasonication		String → sulfidization → ultrasonic → pH adjustment → xanthate adsorption → flotation

The pH values were adjusted to  $10 \pm 0.05$ ; the time for sulfidization and xanthate adsorption was 3 min. For the washed group, the sulfidized sample was washed with deionized water three times, and then mixed with fresh deionized water.

2.4. EPMA measurements

To analyze the location of O and S, EPMA was undertaken using EPMA-1720 Series (Shimadzu corporation) equipped with four wavelength dispersive spectrometer (WDS) detectors.

Besides two powder samples that were labeled as a and b, we prepared a cross-sectional specimen of sulfidized malachite particles (sample c) as follows: the sulfidized malachite particles were mixed with epoxies. After curing, the sample was polished with emery paper and cleaned with deionized water. Before measurement, the samples were coated with carbon.

2.5. XRD studies

XRD studies were performed using an X'Pert3 Powder XRD system with CuK $\alpha$  radiation ( $\lambda = 1.5406 \text{ \AA}$ ; scanning speed:  $0.2^\circ/\text{s}$ ). To determine the crystal phase of the sulfidization product under flotation-related conditions, the sulfidization product was extracted from the sulfidized malachite powders as follows: First, 5 g of sulfidized malachite sample (sulfidized ten times as described in Section 2.3) and 100 mL of leaching agent that contained sulfuric acid (5 g/L) and ascorbic acid (40 g/L) were placed in a beaker to react until  $\text{Cu}_2(\text{OH})_2\text{CO}_3$  was completely dissolved. Subsequently, the solute was removed by centrifugation and washed with absolute ethanol six times. Lastly, the solid residue from the final wash was dried at  $40^\circ\text{C}$  to obtain the sulfidization product for XRD studies.

2.6. XPS analyses

The sulfidized and unsulfidized malachite samples were studied using a PHI5000 VersaProbe II instrument (ULVAC-PHI, Japan) with an Al K $\alpha$  X-ray source. The operating parameters were as follows: operating voltage = 15 kV, power = 50 W, and pass energy = 46.95 eV. The recorded spectra were calibrated on the basis of the C1s peak at 284.80 eV.

3. Results and discussion

3.1. Flotation tests

Fig. 1 shows the flotation recovery of unsulfidized and sulfidized malachite as a function of the NaBX concentration. With increasing concentration of the NaBX, the flotation recovery of both the unsulfidized and the treated with  $5 \times 10^{-4} \text{ mol/L Na}_2\text{S}$  solution

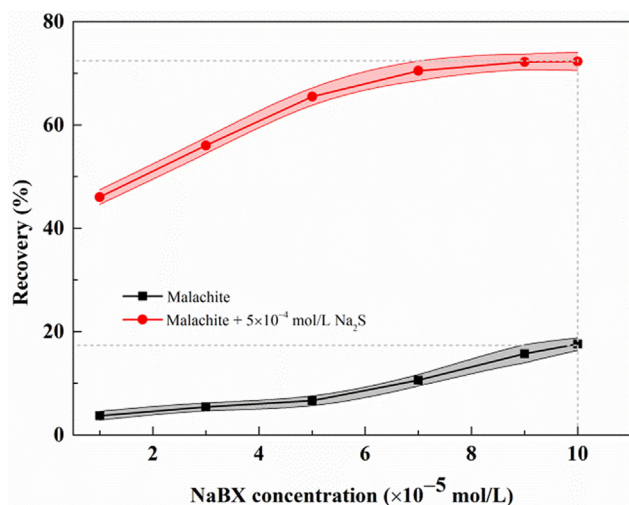


Fig. 1. Flotation recovery of unsulfidized and sulfidized malachite as a function of the NaBX concentration.

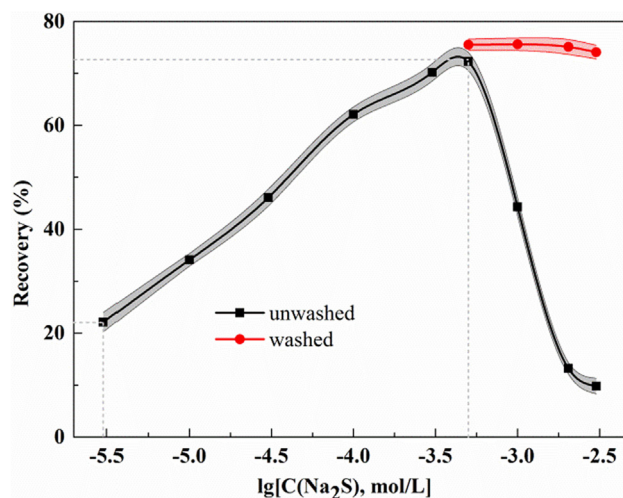


Fig. 2. Flotation recovery of washed and unwashed malachite with  $1 \times 10^{-4} \text{ mol/L Na}_2\text{S}$  as a function of the sodium sulfide concentration.

significantly increased. This figure clearly shows that the recovery of sulfidized malachite was significantly higher than that of the unsulfidized malachite in the concentration range studied.

It is well known that the  $\text{Na}_2\text{S}$  concentration significantly affects the flotation behavior of copper oxide minerals. Fig. 2 shows the flotation recovery of washed and unwashed malachite as a function of the sodium sulfide concentration. For the unwashed malachite samples, the flotation recovery greatly increased, as the  $\text{Na}_2\text{S}$  concentration increased until  $5 \times 10^{-4} \text{ mol/L}$ ; however, the flotation recovery dropped sharply above this optimum concentration. With excess sodium sulfide, the flotation recovery of the washed samples showed no downward trend and was significantly higher than that of the unwashed samples at the same  $\text{Na}_2\text{S}$  concentration. Similar results have been observed with cerussite (Fuerstenau et al., 1987). Hence, the depression of malachite flotation by excess sulfide ions can be attributed to the residual sulfide species in the liquid.

Fig. 3(a) shows that the malachite particles treated with  $5 \times 10^{-4} \text{ mol/L Na}_2\text{S}$  were immersed in deionized water. After ultrasonication for 5 s, the sulfidization product dropped off the malachite surfaces to form many buff-brown colloidal particles (Fig. 3(b)). Flotation tests were conducted to investigate the effect of ultrasonication on the flotation recovery of sulfidized malachite. As shown in Fig. 3(c), the sulfidized malachite particles lost their good floatability after ultrasonication. The recovery of the unsulfidized malachite was also higher

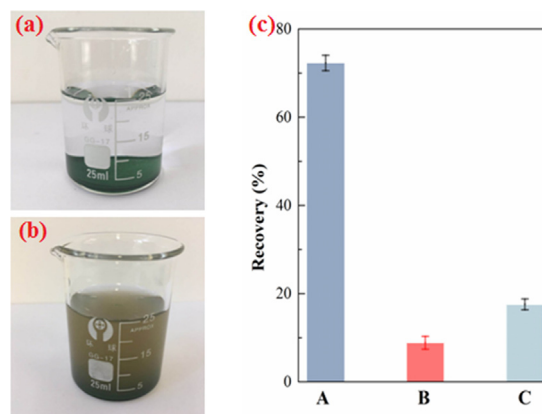


Fig. 3. (a) Image of sulfidized malachite before and (b) after ultrasonication for 5 s. (c) Effect of ultrasonication on flotation recovery of sulfidized malachite with  $1 \times 10^{-4} \text{ mol/L Na}_2\text{S}$ ; (A) sulfidization without ultrasonication, (B) sulfidization with ultrasonication, (C) without sulfidization.

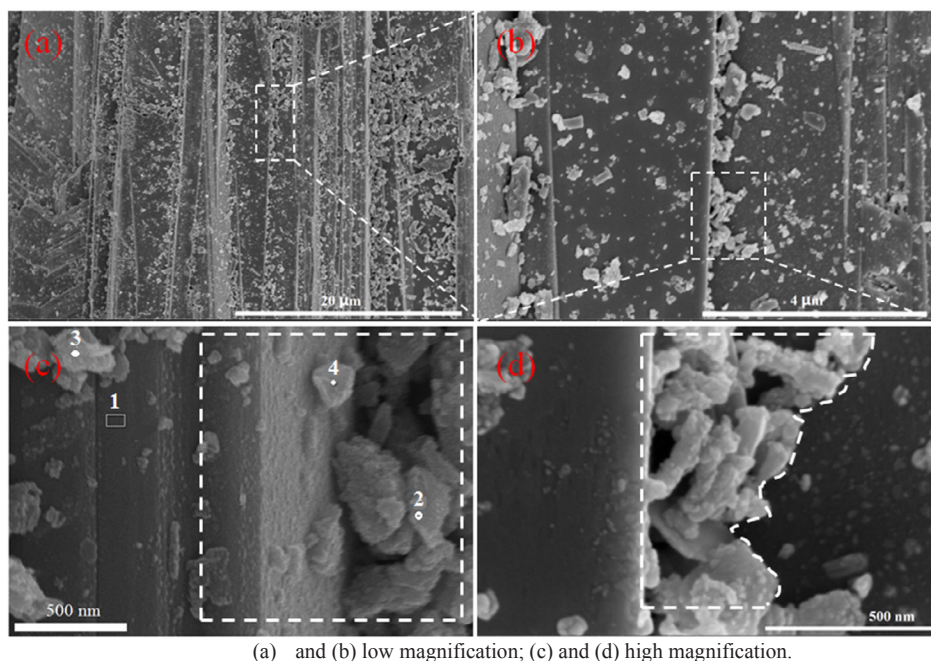


Fig. 4. FESEM images of malachite particles sulfidized with  $5 \times 10^{-4}$  mol/L  $\text{Na}_2\text{S}$ .

than that of sulfidized malachite with ultrasonication; a possible explanation for this might be that the sulfidization product interacted more easily with the collector. These findings indicated that the sulfidization product of malachite is buff-brown and has a colloidal particle size.

### 3.2. FESEM-EDS analyses

FESEM-EDS analyses were performed to observe the sulfidization product. As shown in Fig. S1 (see the Supporting Information), the unsulfidized malachite particles were columnar, and the cleavage stripes were clearly visible. Many tiny grains were found on the particles surfaces. Fig. 4 shows the morphology of the malachite particles sulfidized with  $5 \times 10^{-4}$  mol/L  $\text{Na}_2\text{S}$ . Under low magnification (Fig. 4(a) and 4(b)), no significant differences were found between the sulfidized and unsulfidized malachite. However, a significant change in surface morphology was observed under high magnification. The malachite surface was coated with a layer of mud-like material in the marked areas (Fig. 4(c) and (d)). In addition, the EDS analyses revealed that the chemical composition of the marked areas differed from those of the surrounding areas. Fig. 5(a) shows that the Cu concentration of Spot 1 in Fig. 4(c) (the surrounding area) is 54.9%, which is close to the theoretical value (57.47%); its O concentration is 31% and no S is detected. However, other EDS results (Fig. 5(b), (c) and (d)) indicated that the areas that were coated with mud-like materials contained sulfur. Thus, it can be concluded that the mud-like material was solid product for malachite sulfidization. Moreover, it can be tentatively suggested that the thickness of the sulfidization product layer was well below  $1 \mu\text{m}$ , based on its O to S concentration ratio and the sample depth for EDS analysis.

With a high  $\text{Na}_2\text{S}$  concentration ( $3 \times 10^{-3}$  mol/L), the morphology changes were more noticeable. It could be clearly observed that a large amount of sulfidization product was coated on the malachite surface (see Fig. S2).

These FESEM images clearly showed the heterogeneous distribution of sulfidization product of malachite, which appeared to preferentially grow on specific areas such as the slit, crystal edges or tiny crystal grains. In addition, these images highlighted that the sulfidization product is a solid multilayer.

### 3.3. EPMA measurements

EPMA mapping was used to further confirm the heterogeneous distribution of the sulfidization product. Fig. 6(a) and (b) presents secondary electron images of the sulfidized malachite particles and their corresponding WDS elemental mapping. A heterogeneous sulfur distribution was observed in the both particles samples that were sulfidized with  $5 \times 10^{-4}$  and  $3 \times 10^{-3}$  mol/L  $\text{Na}_2\text{S}$  solution, respectively. Moreover, more sulfur distribution was observed when treated with high  $\text{Na}_2\text{S}$  concentration; the results also showed the sulfidization product preferentially grew on the slit, fractures and crystal edges, suggesting that the surface microstructure of malachite particles played a significant role during sulfidization.

Predictably, at higher  $\text{Na}_2\text{S}$  concentration, more sulfidization products grew on malachite to form  $\text{Cu}_2(\text{OH})_2\text{CO}_3$ /copper sulfide core-shell structure. As shown in Fig. 6(c), oxygen was observed inside the particles while sulfur was found localized in the outer surfaces of malachite particles, clearly showing an oxygen-containing core and a sulfur-containing shell. In addition, the thickness of sulfidization product layer was measured with the use of EPMA-1720 Analysis software; and the measurement results (see Fig. S3 and Table S1) show that the thickness of sulfidization product shell ranged from 0.98 to  $3.41 \mu\text{m}$  and averaged  $2.32 \mu\text{m}$ .

### 3.4. XRD studies

The sulfidization product is an important part of a study on the sulfidization mechanism of malachite. Determination of the sulfidization product is required to determine the sulfidization mechanism. Thus, there were limitations to understanding the sulfidization flotation of malachite. To determine the crystal phase of sulfidization product, XRD studies were performed. Fig. 7 shows XRD patterns of unsulfidized and sulfidized malachite. Peaks of unsulfidized malachite sample (Fig. 7(a)) could be indexed to malachite  $\text{Cu}_2(\text{OH})_2\text{CO}_3$  (JCPDS No.41-1390), and a few very weak impurity peaks were observed, confirming the high purity of malachite sample. However, there were no differences between the three XRD patterns, and no characteristic peaks of the sulfidization product were found for either of the sulfidized malachite samples (Fig. 7(b) and (c)). The results showed

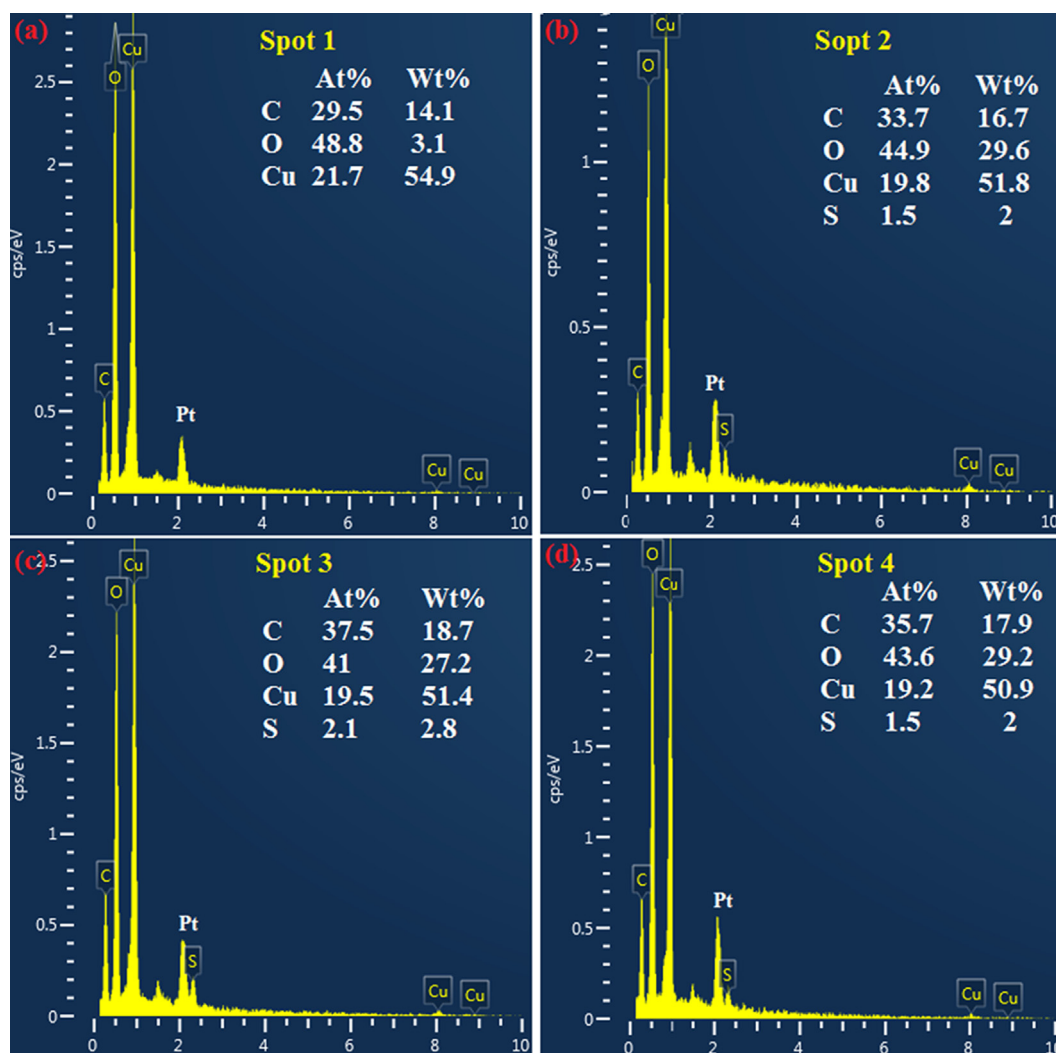


Fig. 5. EDS results corresponding to Fig. 4(c).

that the amount of sulfidization product was insufficient to be detected.

As malachite was dissolved in sulfuric acid while the sulfide was not, we extracted the sulfidization product from the sulfidized malachite. The color of the extracted sulfidization product (Fig. 8(a)) matched that of the colloid shown in Fig. 3(b). Fig. 8(b) presents the XRD pattern of the extracted sulfidization products. When the sodium sulfide concentration was  $5 \times 10^{-4}$  mol/L, the XRD pattern showed that the sulfidization product comprised  $\text{Cu}_{31}\text{S}_{16}$  (djurleite) and  $\text{Cu}_7\text{S}_4$  (anilite). It was difficult to perform semi-quantitative analysis of the two crystal phases, since their patterns closely overlapped. However, it could still be inferred that  $\text{Cu}_{31}\text{S}_{16}$  was the main crystal phase. When the sodium sulfide concentration was  $3 \times 10^{-3}$  mol/L, the sulfidization product also comprised  $\text{Cu}_{31}\text{S}_{16}$  (djurleite) and  $\text{Cu}_7\text{S}_4$  (anilite), yet the proportion of  $\text{Cu}_{31}\text{S}_{16}$  (djurleite) increased. Furthermore, the broad and weak peaks indicated that the sulfidization products had a fine crystal grain, which was consistent with the characteristics of colloidal particles.

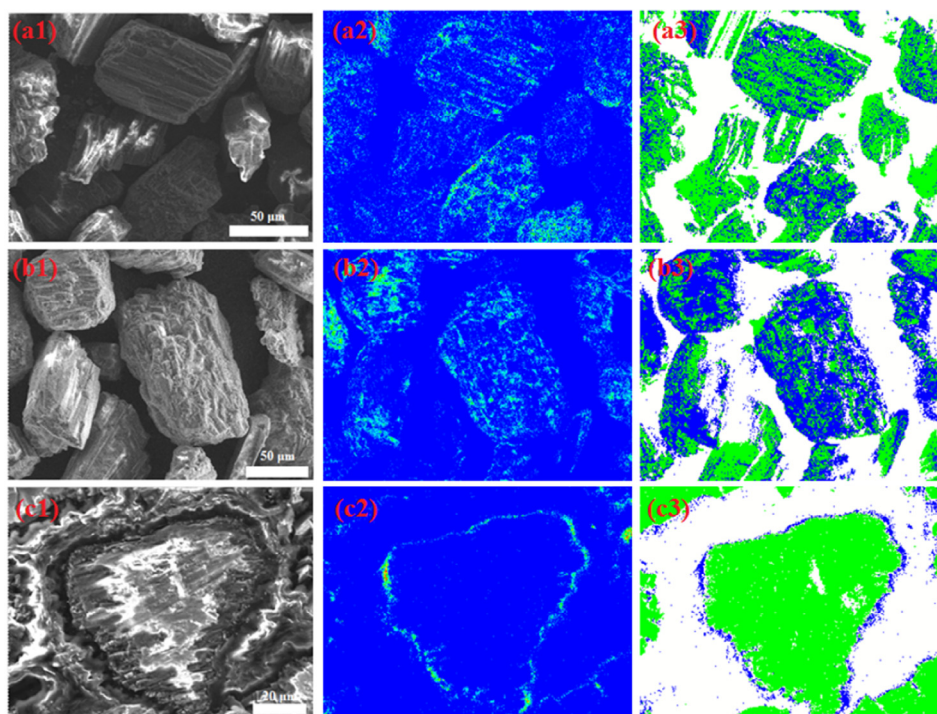
To the best of our knowledge, this is the first study that determines the crystal phase of sulfidization product of malachite under flotation-related conditions. Both djurleite ( $\text{Cu}_{31}\text{S}_{16}$ ) and anilite ( $\text{Cu}_7\text{S}_4$ ) are compounds of the chalcocite group, represented by  $\text{Cu}_{2-x}\text{S}$  ( $0 \leq x \leq 0.6$ ), and their other chemical formula are  $\text{Cu}_{1.97-1.94}\text{S}$  and  $\text{Cu}_{1.75}\text{S}$ , respectively. In addition, six other compounds of the  $\text{Cu}_{2-x}\text{S}$  chalcocite group exist, namely,  $\gamma$ -chalcocite  $\text{Cu}_2\text{S}$  (low orthorhombic),  $\beta$ -chalcocite  $\text{Cu}_2\text{S}$  (high hexagonal), digenite  $\text{Cu}_{1.80}\text{S}$ , roxbyite  $\text{Cu}_{1.78}\text{S}$ , geerite  $\text{Cu}_{1.60}\text{S}$  and spionkopite  $\text{Cu}_{1.40}\text{S}$  (Cheng et al., 2008; Zhao et al.,

2009). Since there are many kinds of phases in the copper–sulfur system, more conditions such as pH and the oxidation–reduction potential need to be considered in the future. The method of purifying the sulfidization product, which is inspired by the chemical phase analysis, will continue to play an essential role.

### 3.5. XPS analyses

The XRD results indicated a transformation of solid  $\text{Cu}_2^{\text{II}}(\text{OH})_2\text{CO}_3$  to  $\text{Cu}_{2-x}\text{S}$ , suggesting that the sulfidization reaction involves an oxidation–reduction process. XPS is a sensitive and widely used surface analysis technique that can provide much information on sample surfaces such as the composition, concentration and chemical states of elements. Thus, XPS analyses were implemented to characterize the surface states of unsulfidized and sulfidized malachite. Fig. 9 shows the C1s, O1s, Cu2p, and S2p spectra of unsulfidized and sulfidized malachite samples.

As shown in Fig. 9(a1), the recorded C1s spectrum of the unsulfidized malachite sample was fitted with three contributions: the first peak labeled C<sub>1</sub> at 284.80 eV was assigned to C–C, C = C, and C–H, and the second peak labeled C<sub>2</sub> at 286.21 eV was attributed to C – O single bonds (Frateur et al., 2007; Wang et al., 2017); this two peaks were attributed to adventitious carbon. The third peak labeled C<sub>3</sub> at 289.43 eV was attributed to O = C – O, i.e., carbonate in the malachite lattice (Feng et al., 2017). For the two sulfidized samples, both two C1s



(a1), (b1) and (c1) secondary electron images; (a2), (b2) and (c2) S elemental mapping; (a3), (b3) and (c3) overlays of O (green) and S (blue) elemental mapping.

**Fig. 6.** EPMA surface scan of malachite particles sulfidized with (a)  $5 \times 10^{-4}$  and (b)  $3 \times 10^{-3}$  mol/L  $\text{Na}_2\text{S}$  solution. (c) EPMA surface scan of the cross-sectional specimen of malachite particles sulfidized with  $6 \times 10^{-3}$  mol/L  $\text{Na}_2\text{S}$  solution.

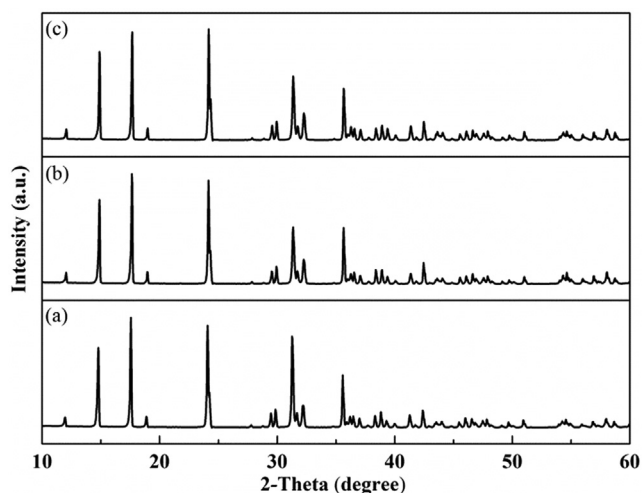


**Fig. 7.** XRD patterns of malachite that treated with (a) 0, (b)  $5 \times 10^{-4}$  and (c)  $3 \times 10^{-3}$  mol/L  $\text{Na}_2\text{S}$  solution.

signals were also fitted as adventitious carbon and carbonate.

The malachite lattice contains two types of O atoms derived from hydroxyl and carbonate. Moreover, O in the contaminants could also contribute to the O1s spectra. However, only one spectral peak was fitted for all the O1s spectra (Fig. 9(b)), and the binding energies of peaks were within the range 531.48–531.71 eV, which is consistent with the studies conducted by Feng et al. (2017).

Fig. 9(c1) presents the Cu 2p spectrum of the unsulfidized malachite sample. This shows the fingerprint of Cu(II) (cupric): a pair of satellite peaks, a  $\text{Cu}2p_{3/2}$  peak at 934.51 eV, and a  $\text{Cu}2p_{1/2}$  peak at 954.31 eV. After treatment with aqueous sodium sulfide solution, new peaks emerged at binding energies of  $932.20 \pm 0.09$  and  $952 \pm 0.09$  eV; meanwhile, the satellite peaks and Cu2p peaks of Cu(II) became weaker

(see Fig. 9(c2) and (c3)). Therefore, there was a change from Cu(II) to Cu(I) (cuprous) species during sulfidization, based on evolution of satellite peaks and the chemical shifts of Cu2p peaks (Li et al., 2015; Meda et al., 2002), which corresponded with our XRD results. Furthermore, previous XPS studies also reported valence changes in malachite sulfidization (Wu et al., 2017; Feng et al., 2017; Shen et al., 2019).

The S2p spectra of the unsulfidized and sulfidized malachite samples are shown in Fig. 9(d1), (d2) and (d3). For the unsulfidized malachite sample, no signal of S was detected (Fig. 9(d1)). After treatment with aqueous sodium sulfide solution, however, the S2p peaks were clearly visible (Fig. 9(d2) and (d3)). The S2p spectrum (Fig. 9(d2)) of the sample sulfidized with  $5 \times 10^{-4}$  mol/L  $\text{Na}_2\text{S}$  was fitted with two contributions: the first, with binding energies of 161.61 eV for the  $\text{S}2p_{3/2}$  level and 162.79 eV for the  $\text{S}2p_{1/2}$  level, was ascribed to the divalent sulfide ion ( $\text{S}^{2-}$ ); the second, with binding energy of 163.87 eV for the  $\text{S}2p_{3/2}$  level and 165.05 eV for the  $\text{S}2p_{1/2}$  level, was attributed to the polysulfide ion ( $\text{S}_n^{2-}$ ,  $n \geq 2$ ) (Wu et al., 2017). When  $\text{Na}_2\text{S}$  concentration was  $3 \times 10^{-3}$  mol/L, both divalent sulfide and polysulfide were also observed (Fig. 9(d3)). Because no polysulfides were observed in the previous XRD studies, it was considered that polysulfide resulted from slight oxidation of sulfidization product surfaces.

Table 2 compares the atomic concentrations of malachite samples sulfidized with different  $\text{Na}_2\text{S}$  concentrations. As sodium sulfide concentration increased, the concentrations of C and O decreased while those of Cu and S increased, which were also neatly illustrated by Fig. 9. By combining these results with the percentage data for various contributions, it can be concluded that as the sodium sulfide concentration increased, the concentrations of carbonate, hydroxyl, and Cu(II) species decreased whereas those the concentration of Cu(I) species and sulfur increased. After sulfidization, the increase in the total Cu concentration on the malachite surfaces was because  $\text{Cu}_{2-x}\text{S}$  had a higher copper content than  $\text{Cu}_2(\text{OH})_2\text{CO}_3$ . Thus, the XPS results are consistent well with the previous results. However, the EDS results concerning the copper concentration (Fig. 5) are abnormal, which may be due to the

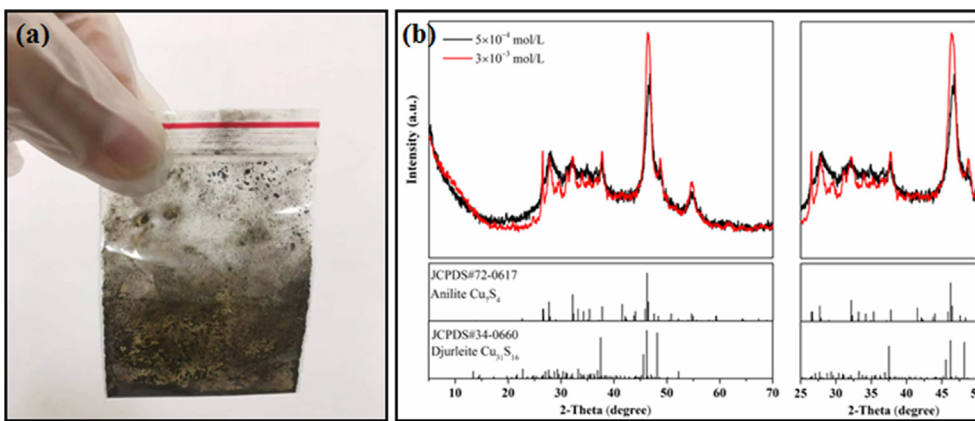


Fig. 8. (a) Image of sulfidization product that was extracted from malachite sample sulfidized with  $3 \times 10^{-3}$  mol/L  $\text{Na}_2\text{S}$ . (b) XRD patterns of sulfidization products that were extracted from the malachite sulfidized with  $5 \times 10^{-4}$  and  $3 \times 10^{-3}$  mol/L  $\text{Na}_2\text{S}$ .

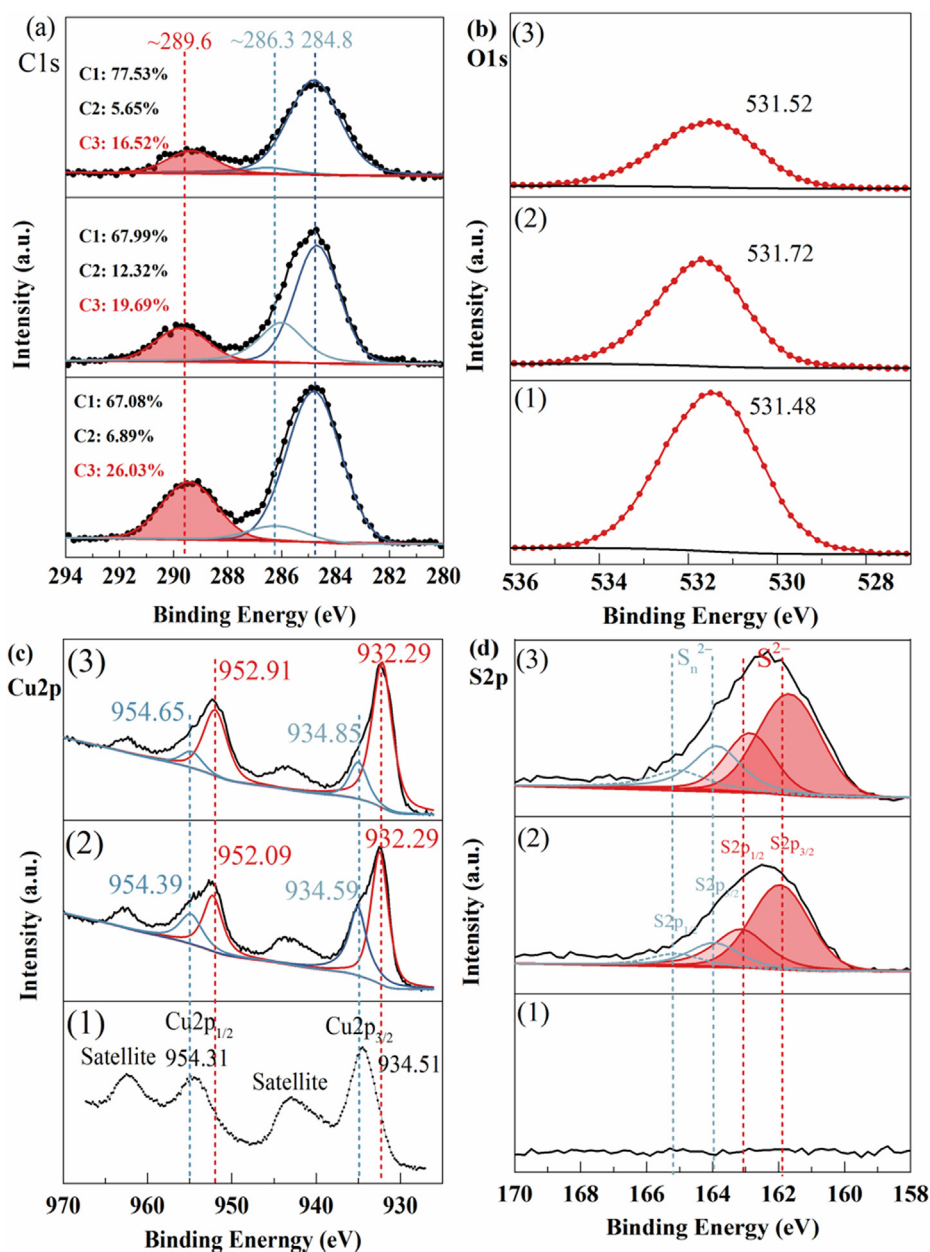


Fig. 9. XPS spectra of (a) C1s, (b) O1s, (c) Cu2p and (d) S2p of (1) unsulfidized malachite and treated with (2)  $5 \times 10^{-4}$  and (3)  $3 \times 10^{-3}$  mol/L  $\text{Na}_2\text{S}$ .

**Table 2**

Atomic concentrations of malachite samples treated with (a) 0, (b)  $5 \times 10^{-4}$  and (c)  $3 \times 10^{-3}$  mol/L  $\text{Na}_2\text{S}$ .

Samples	Atomic concentrations, %					
	C	O	S	Total Cu	Cu(II)	Cu(I)
a	38.99	48.33	< 0.1	12.68	12.68	—
b	36.69	38.16	8.49	16.66	6.98	9.68
c	33.36	31.82	16.39	18.43	2.94	15.49

topography or spray platinum treatment.

### 3.6. Sulfidization mechanism

Based on the above characterizations and analyses, it can be concluded that sulfidization of malachite is a heterogeneous solid–liquid reaction in which the solid product attaches to the unreacted malachite. Sulfidization is a phase transition from  $\text{Cu}_2(\text{OH})_2\text{CO}_3$  to  $\text{Cu}_{2-x}\text{S}$  on malachite surfaces, which is driven by their solubility difference. The sulfidization product on malachite is not a monolayer but a solid multilayer. Hence, sulfidization initially occurs at the malachite–aqueous solution interface, and then proceeds into the bulk of the solid particles, at the newly formed solid–solid ( $\text{Cu}_2(\text{OH})_2\text{CO}_3/\text{Cu}_x\text{S}_y$ ) solution interface. Sulfidization process involves the diffusion, adsorption and chemical reaction; e.g., sulfidization at the solid–solid interface must involve diffusion of  $\text{HS}^-$  from solution through the newly formed solid copper sulfide phase, and diffusion of carbonate ions and hydroxyl ions from the crystal lattice of malachite, through the copper sulfide layer, and into solution.

From another viewpoint, sulfidization is a crystallization process that involves heterogeneous nucleation followed by growth of the nuclei (He and Li, 2007). Fig. 10 shows a schematic diagram of a sulfidized malachite particle at the optimum sodium sulfide concentration. Because the copper sulfide nuclei formed preferentially in the regions with high reactivity, the sulfidization reaction was localized and the sulfidization product was heterogeneously distributed under flotation-related condition. Fig. 11 highlights the microstructural variations during malachite sulfidization. During this process, the malachite lattice was destroyed, while copper sulfide lattices were formed. The copper sulfide grown on the unreacted malachite radically changed the surface properties of the mineral particles, rendering malachite amenable to xanthate flotation. Previous studies revealed that sulfidized oxide-type minerals also exhibited flotation behavior that was

dependent on the pulp potential (Castro et al., 1974b; Herrera-Urbina et al., 1999). This study facilitates better understand the interaction between sulfidized malachite particles and collectors. This is essentially a reaction of  $\text{Cu}_{2-x}\text{S}$  grown on malachite with xanthate, which must also be controlled by the electrochemical mechanism (Hanson and Fuerstenau, 1991). As well known, the dissolved oxygen in pulp is required for the flotation of sulfide compounds with xanthates; however, the dissolved oxygen in pulp can be lost as a result of the oxidation of sulfidizing agents. A simple and effective method, i.e. aerating agitation for some time after sulfidization and before the addition of collector, can be performed to further improve the sulfidization flotation performance of copper oxide minerals. With higher  $\text{Na}_2\text{S}$  concentration, more sulfidization products grew on malachite to form  $\text{Cu}_2(\text{OH})_2\text{CO}_3/\text{copper sulfide}$  core–shell structure; thus, sulfidization of malachite surfaces with aqueous sodium sulfide solutions may well be represented by the well known “shrinking core model”. However, the copper sulfide grown on malachite can block the further sulfidization of the unreacted core so that excess sulfide species that remain in aqueous solution depress the flotation of malachite. When the excess sulfide species in aqueous solution are eliminated, the sulfidized malachite is naturally restored to its floatability. Incidentally, solution conditions such as the pulp pH, sodium sulfide concentration and solvent may affect the nucleation and growth of sulfidization product, then effect on the sulfidization flotation performance. For example, we speculate that the growth rate of sulfidization product is high at high concentration of sodium sulfide, which is detrimental to the stability of the sulfidization product on malachite surfaces. That might be the reason why sodium sulphide is added in stages in actual practice, rather than adding as one consolidated dosage.

What is striking about our findings is that the solid products, djurleite and anilite, were the copper-deficient compounds, suggesting that some Cu(II) was reduced to Cu(I) during sulfidization. Because only divalent sulfide ions exhibited reducibility in the reaction system, these were the most likely reductant for reduction of Cu(II). In fact, this reduction of Cu(II) to Cu(I) by sulfide was observed by Luther et al. (2002), Kuchar et al. (2006), and Ma et al. (2014). Decades ago, Castro and his colleagues discovered the formation of  $\text{S}_2\text{O}_3^{2-}$  during the sulfidization of synthetic tenorite and chrysocolla (Castro et al., 1974a; Castro et al., 1974b); Under the oxygen-deprived conditions, some sulfide was oxidized to sulfate during the sulfidization of copper oxide nanoparticles (Ma et al., 2014). Thus, we conclude that sulfide ions play dual roles during sulfidization of malachite: some, as reductant, were oxidized to sulfoxy species ( $\text{S}_y\text{O}_z^{2-}$ ) such as sulfate ( $\text{SO}_4^{2-}$ ), sulfite ( $\text{SO}_3^{2-}$ ) and thiosulfate ( $\text{S}_2\text{O}_3^{2-}$ ) ions, contributing to the reduction of

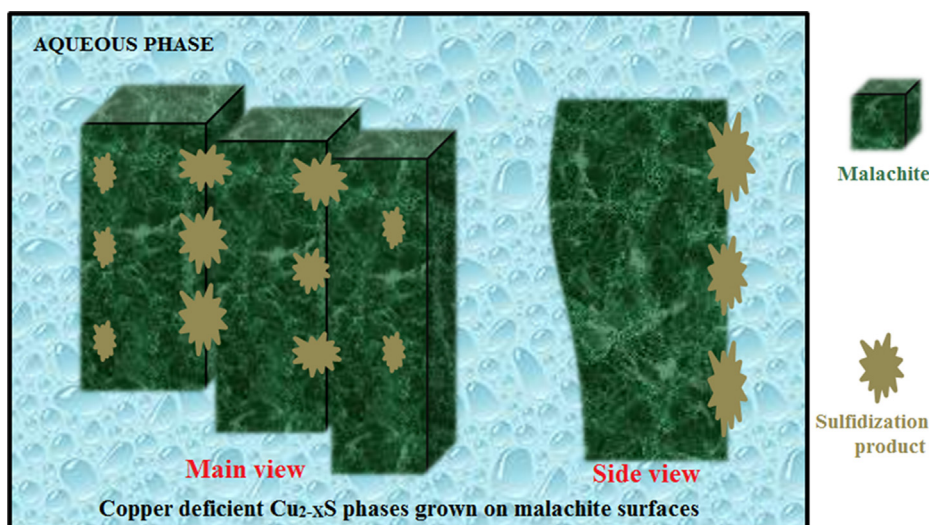


Fig. 10. Schematic diagram of the sulfidized malachite particle at the optimum sodium sulfide concentration.

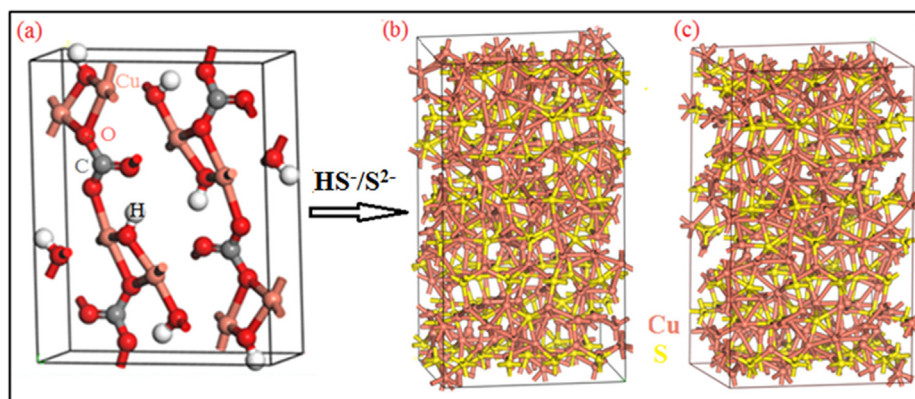
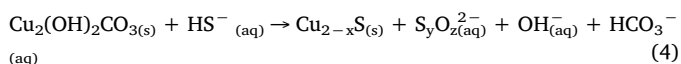


Fig. 11. Microstructural variations during sulfidization. Unit cell crystal models of (a) malachite, (b) djurleite, and (c) anilite.

Cu(II) to Cu(I); others, as sulfidizing agent, occurred chemically combined with the newly formed Cu(I) to form copper(I) sulfide. As well, sulfidization also involves the diffusion of newly formed sulfoxy ions through the copper sulfide phase, and into solution. Based on the hard–soft acid–base (HSAB) principles,  $S^{2-}$  (soft Lewis base) exhibits a stronger binding with  $Cu^+$  (soft Lewis acid) than  $Cu^{2+}$  (medium Lewis acid), which thermodynamically favors the formation of  $Cu_2S$ . Notably, this tendency is also illustrated by the lower Gibbs free energy and solubility product of  $Cu_2S$  compared to  $CuS$  ( $\Delta_f G(Cu_2S) = -86.2 \text{ kJ}\cdot\text{mol}^{-1}$  vs  $\Delta_f G(CuS) = -53.7 \text{ kJ}\cdot\text{mol}^{-1}$ ;  $K_{sp}(Cu_2S) = 10^{-47.8}$  vs  $K_{sp}(CuS) = 10^{-35.06}$ ) (Wu et al., 2019). Interestingly, the copper-deficient  $Cu_{2-x}S$  phases has a thermodynamic stability toward the  $Cu_2S$  under ambient conditions (Lukashev et al., 2007; Zhao et al., 2009). Based on the above discussion, it can be concluded that this thermodynamically favors the formation of the copper-deficient  $Cu_{2-x}S$  phases in sulfidization of malachite or other copper oxide minerals such as azurite. According to our findings, malachite sulfidization can be described as follows:



#### 4. Conclusions

Sulfidization of malachite is a heterogeneous solid–liquid reaction in which the solid sulfidization product attaches to the unreacted malachite. It is a phase-transition process driven by the magnitude solubility difference between  $Cu_2(OH)_2CO_3$  and  $Cu_{2-x}S$ . The sulfidization reaction thermodynamically favors the formation of the copper-deficient  $Cu_{2-x}S$  phases. Sulfide ions play dual roles during sulfidization: some, as reductant, were oxidized to sulfoxy ( $S_yO_z^{2-}$ ) species, contributing to the reduction of Cu(II) to Cu(I); while others, as sulfidizing agent, occurred chemically combined with the newly formed Cu(I) to form copper(I) sulfide.

The formation of  $Cu_{2-x}S$  on malachite surfaces involves heterogeneous nucleation followed by growth of the nuclei. Because the copper sulfide nuclei form preferentially in the regions with high reactivity, the sulfidization reaction is localized and copper sulfide is heterogeneously distributed under flotation-related conditions. Thus, the surface microstructure of the mineral particles plays a significant role during sulfidization.

The copper sulfide grown on malachite radically changed the surface properties of the mineral particles, which rendered malachite amenable to the xanthate flotation.

#### CRediT authorship contribution statement

Ruizeng Liu: Investigation, Formal analysis, Writing - original

draft. Dianwen Liu: Funding acquisition. Jialei Li: Conceptualization, Data curation, Formal analysis, Investigation, Methodology. Jianmin Li: Resources, Data curation. Zhicheng Liu: Resources, Methodology. Xiaodong Jia: Data curation. Shengwang Yang: Resources. Jiangli Li: Investigation. Shuai Ning: Investigation.

#### Declaration of Competing Interest

The authors declare that they have no known competing financial interests or personal relationships that could have appeared to influence the work reported in this paper.

#### Acknowledgements

The authors sincerely thank the National Natural Science Foundation of China (Grant No. 51264019), National Basic Research Program of China (973 Program, Grant No. 2014CB643404) for financial support. We also thank to Chengyu Yang from shiyanjia lab (www.shiyanjia.com) for the FESEM measurements.

#### Appendix A. Supplementary material

Supplementary data to this article can be found online at <https://doi.org/10.1016/j.mineng.2020.106420>.

#### References

- Bustamante, H., Castro, S., 1975. Hydrophobic effects of sodium sulfide on malachite flotation. *Trans. IMM* 84, 167–171.
- Castro, S., Goldfarb, J., Laskowski, J., 1974a. Sulphidizing reactions in the flotation of oxidized copper minerals, I. chemical factors in the sulphidization of copper oxide. *Int. J. Miner. Process.* 33, 1(2), 141–149. [https://doi.org/10.1016/0301-7516\(74\)90010-6](https://doi.org/10.1016/0301-7516(74)90010-6).
- Castro, S., Soto, H., Goldfarb, J., Laskowski, J., 1974b. Sulphidizing reactions in the flotation of oxidized copper minerals, II. role of the adsorption and oxidation of sodium sulphide in the flotation of chrysocolla and malachite. *Int. J. Miner. Process.* 1(2), 151–161. [https://doi.org/10.1016/0301-7516\(74\)90011-8](https://doi.org/10.1016/0301-7516(74)90011-8).
- Cheng, H.N., Hu, Y.H., Gao, J., Heng, M.A., 2008. Bioleaching of anilite by *acidithiobacillus ferrooxidans*. *Trans. Nonferrous Met. Soc. China* 18 (6). [https://doi.org/10.1016/S1003-6326\(09\)60017-0](https://doi.org/10.1016/S1003-6326(09)60017-0).
- Fuerstenau, M.C., Olivas, S.A., Herrera-Urbina, R., Han, K.N., 1987. The surface characteristics and flotation behavior of anglesite and cerussite. *Int. J. Miner. Process.* 20, 73–85.
- Frature, I., Lecoer, J., Zanna, S., Olsson, C.O.A., Landolt, D., Marcus, P., 2007. Adsorption of BSA on passivated chromium studied by a flow-cell EQCM and XPS. *Electrochim. Acta* 52 (27), 7660–7669. <https://doi.org/10.1016/j.electacta.2006.12.060>.
- Feng, Q., Zhao, W., Wen, S., Cao, Q., 2017. Copper sulfide species formed on malachite surfaces in relation to flotation. *J. Ind. Eng. Chem.* 48, 125–132. <https://doi.org/10.1016/j.jiec.2016.12.029>.
- Herrera-Urbina, R., Sotillo, F.J., Fuerstenau, D.W., 1999. Effect of sodium sulfide additions on the pulp potential and amyl xanthate flotation of cerussite and galena. *Int. J. Miner. Process.* 55 (3), 157–170. [https://doi.org/10.1016/S0301-7516\(98\)00029-5](https://doi.org/10.1016/S0301-7516(98)00029-5).
- Han, H., Sun, W., Hu, Y., Baoliang, Jia, B., Tang, H., 2014. Anglesite and silver recovery from jarosite residues through roasting and sulfidization-flotation in zinc

- hydrometallurgy. *J. Hazard. Mater.*, 278(6), 49–54. <https://doi.org/10.1016/j.jhazmat.2014.05.091>.
- He, Y., Li, K., 2007. Novel Janus  $\text{Cu}_2(\text{OH})_2\text{CO}_3/\text{CuS}$  microspheres prepared via a Pickering emulsion route. *J. Colloid Interface Sci.* 306 (2), 296–299. <https://doi.org/10.1016/j.jcis.2006.10.070>.
- Hanson, J.S., Fuerstenau, D.W., 1991. The electrochemical and flotation behavior of chalcocite and mixed oxide/sulfide ores. *Int. J. Miner. Process.* 33 (1–4), 33–47. [https://doi.org/10.1016/0301-7516\(91\)90041-G](https://doi.org/10.1016/0301-7516(91)90041-G).
- Ke, Y., Chai, L.Y., Min, X.B., Tang, C.J., Zhou, B.S., Chen, J., 2015. Behavior and effect of calcium during hydrothermal sulfidation and flotation of zinc-calcium-based neutralization sludge. *Miner. Eng.* 74 68–78. <https://doi.org/10.1016/j.mineng.2015.01.012>.
- Kuchar, D., Fukuta, T., Onyango, M. S., & Matsuda, H., 2006. Sulfidation treatment of copper-containing plating sludge towards copper resource recovery. *J. Hazard. Mater.*, 138(1), 86–94. <https://doi.org/10.1016/j.jhazmat.2006.05.037>.
- Luther, G.W., Theberge, S.M., Rozan, T.F., 2002. Aqueous copper sulfide clusters as intermediates during copper sulfide formation. *Environ. Sci. Technol.* 36 (3), 394–402. <https://doi.org/10.1021/es010906k>.
- Lukashev, P., Lambrecht, W.R.L., Kotani, T., 2007. Electronic and crystal structure of  $\text{Cu}_{2-x}\text{S}$ : Full-potential electronic structure calculations. *Phys. Rev. B* 76 (19) 195202. <https://doi.org/10.1103/PhysRevB.76.195202>.
- Liu, D., 2007. A study on mechanisms of malachite sulfidization and novel flotation technology of copper oxide ores. (Doctoral dissertation. Kunming University of science and technology, China).
- Li, Y., Kawashima, N., Li, J., Chandra, A.P., Gerson, A.R., 2013. A review of the structure, and fundamental mechanisms and kinetics of the leaching of chalcopyrite. *Adv. Colloid Interface Sci.* 197–198 (9), 1–32. <https://doi.org/10.1016/j.cis.2013.03.004>.
- Li, Y., Qian, G., Li, J., Gerson, A.R., 2015. Kinetics and roles of solution and surface species of chalcopyrite dissolution at 650 mV. *Geochim. Cosmochim. Acta* 161, 188–202. <https://doi.org/10.1016/j.gca.2015.04.012>.
- Meda, L., Ranghino, G., Moretti, G., Cerofolini, G.F., 2002. XPS detection of some redox phenomena in Cu-zeolites. *Surf. Interface Anal.* 33 (6), 516–521. <https://doi.org/10.1002/sia.1228>.
- Ma, R., Stegemeier, J., Levard, Clément, Dale, J.G., Noack, C.W., Yang, T., 2014. Sulfidation of copper oxide nanoparticles and properties of resulting copper sulfide. *Environ. Sci.: Nano* 1 (4), 347. <https://doi.org/10.1039/c4en00018h>.
- Shen, P., Liu, D., Zhang, X., 2019. Effect of  $(\text{NH}_4)_2\text{SO}_4$  on eliminating the depression of excess sulfide ions in the sulfidization flotation of malachite. *Miner. Eng.* 137, 43–52. <https://doi.org/10.1016/j.mineng.2019.03.015>.
- Thompson, M., 2006. *Base Metals Handbook*. Woodhead Publishing Pages 3-1-3-77.
- Wang, J., Lu, J., Zhang, Q., Saito, F., 2003. Mechanochemical sulfidization of nonferrous metal oxides by grinding with sulfur and iron. *Ind. Eng. Chem. Res.* 42 (23). <https://doi.org/10.1021/ie030046b>.
- Wu, D., Ma, W., Mao, Y., Deng, J., Wen, S., 2017. Enhanced sulfidation xanthate flotation of malachite using ammonium ions as activator. *Sci. Rep.* 7 (1), 2086. <https://doi.org/10.1038/s41598-017-02136-x>.
- Wang, W., Zhao, Y., Hui, L., Song, S., 2017. Fabrication and mechanism of cement-based waterproof material using silicate tailings from reverse flotation. *Powder Technol.*, 315, 422–429. <https://doi.org/10.1016/j.powtec.2017.04.029>.
- Wu, X., Markir, A., Ma, L., Xu, Y., 2019. A four-electron sulfur electrode hosting  $\text{Cu}_2 + \text{Cu} +$  redox charge carrier. *Angew. Chem.* 2019 (131), 12770–12775. <https://doi.org/10.1002/ange.201905875>.
- Zhou, R., Chander, S., 1993. Kinetics of sulfidization of malachite in hydrosulfide and tetrasulfide solutions. *Int. J. Miner. Process.* 37 (3), 257–272. [https://doi.org/10.1016/0301-7516\(93\)90030-E](https://doi.org/10.1016/0301-7516(93)90030-E).
- Zhao, Y., Pan, H., Lou, Y., Qiu, X., Burda, C., 2009. Plasmonic  $\text{Cu}_{2-x}\text{S}$  nanocrystals: optical and structural properties of copper-deficient copper(I) sulfides. *J. Am. Chem. Soc.* 131 (12), 4253–4261. <https://doi.org/10.1021/ja805655b>.